Results in Chemistry 3 (2021) 100254

Contents lists available at ScienceDirect

Results in Chemistry

journal homepage: www.sciencedirect.com/journal/results-in-chemistry

Combining experimental and theoretical approaches to study the structural and spectroscopic properties of Flakka (α-pyrrolidinopentiophenone)

Adrinê Elisabeth Ganimian Tcharkhetian [a,3], Aline Thais Bruni [a,b,1], Caio Henrique Pinke Rodrigues [a,b,2,*]

[a] Departamento de Química, Faculdade de Filosofia, Ciências e Letras de Ribeirão Preto – USP. Avenida Bandeirantes, Monte Alegre, Ribeirão Preto, São Paulo 3900, Brasil

[b] INCT-Forense -Departamento de Química, Faculdade de Filosofia, Ciências e Letras de Ribeirão Preto – USP. Avenida Bandeirantes, Monte Alegre, Ribeirão Preto, São Paulo 3900, Brasil

ARTICLE INFO

Keywords:
Forensic chemistry
New psychoactive substances
Cathinones
α-PVP

ABSTRACT

New Psychoactive Substances (NPS) present several identification and public health challenges. However, experimental studies with illicit substances can involve regulatory restrictions, and obtaining information about them can be time-consuming. In this scenario, in silico methods can help to monitor the emergence of new synthetic substances such as synthetic cathinones, some of the most seized NPS. Here, we study the cathinone alpha-PVP or Flakka by theoretical chemistry methods to evaluate its structure, possible conformers, and spectroscopic profile. Initially, we performed a systematic conformational analysis and an analysis based on the Boltzmann distribution. We determined the most probable experimental structure and compared it to the crystallographic structure, to verify similarity between the forms. Next, we applied the factorial design to the obtained structure so that we could decide on the most adequate computational method to obtain the spectrum in the infrared and NMR region. Then, we compared the results with experimental data available in the literature. Finally, we evaluated multivariate statistical methods to ensure that we would come to conclusions based on the responses of each step. All the steps indicated similarity between the theoretical data and the experimental results when we used the combination DFT B3LYP and the basis 6-31G**. Our results demonstrate the potential application of computer simulation in forensic chemistry and provide valuable spectroscopic and structural information about illegal substances.

Introduction

Synthetic cathinones consist of β-keto-phenylethylamines or β-keto-amphetamines [1]. They can derive from cathinone, a natural alkaloid that occurs in khat leaves (*Catha edulis*), typical of eastern Africa and southern Arabia [1]. The present study deals with α-pyrrolidinopentiophenone (1-Phenyl-2-(1-pyrrolidinyl)pentan-1-one; α-PVP), better known as flakka, a compound belonging to the class of "pyrovalerone cathinones" [2,3]. In 2015, α-PVP was one of the five most apprehended cathinones [4,5].

Analysis of new psychoactive substances (NPS) is challenging because information about these structures is lacking. The fast appearance of these new substances, which are constantly created and introduced into the market, requires new analytical methods because the

Abbreviations: θ_i, Dihedral increment of angle *i*; X, Electronegativity; 6-31G**, Double-zeta plus polarization basis-set Pople's; ANOVA, Analysis of variance; B3LYP, Becke Method, three-parameter, Lee-Yang-Parr; CPCM, Conductor-Like Polarizable Continuum Model; DFT, Density Functional Theory; E_{HOMO}, Highest occupied molecular orbital energy; E_{LUMO}, Lowest unoccupied molecular orbital energy; HCA, Hierarchical Cluster Analysis; KL, Kullback–Leibler Divergence; NMR, Nuclear Magnetic Resonance; NPS, New psychoactive substances; PBE0, Perdew-Burke-Ernzerhof; PCA, Principal Component Analysis; RMSD, Root Mean Square Difference; SWGDRUG, Scientific Working Group for the Analysis of Seized Drugs; TZVP, Triple Zeta Ahlrichs basis set with a single set of polarization functions; UFF, Universal Force Field.

* Corresponding author.
E-mail addresses: adrine.ganimian@gmail.com (A.E.G. Tcharkhetian), aline.bruni@usp.br (A.T. Bruni), caio.pinke.rodrigues@usp.br (C.H.P. Rodrigues).
[1] Aline Thaís Bruni: 0000-0002-7721-3042.
[2] Caio Henrique Pinke Rodrigues: 0000-0002-7794-7484.
[3] Adrinê Elisabeth Ganimian Tcharkhetian: 0000-0001-8092-4753.

https://doi.org/10.1016/j.rechem.2021.100254
Received 20 September 2021; Accepted 25 November 2021
Available online 30 November 2021

Table 1
Decoded matrix for attribution of factors and levels.

Factor	Level	
	(−)	(+)
DFT	B3LYP	PBE0
Basis-set	TZVP	6-31G**
Correction	D3BJ	–

Table 2
Experimental planning with decoded matrix.

Experiment	DFT	Basis-set	Correction
1	–	–	–
2	+	–	–
3	–	+	–
4	+	+	–
5	–	–	+
6	+	–	+
7	–	+	+
8	+	+	+

currently employed methods may not apply to them [6,7]. The properties of these substances are usually unknown. Understanding instrumental conditions, visual characterization, analyte stability, sample preparation, reference standards, and other characteristics is crucial for detecting and recognizing these substances correctly [8-12]. Experimental studies about illicit or non-regulated substances can be costly and involve restricted regulations. Besides that, analysis can be time-consuming [13], may require different analytical tools (such as chromatographic methods and spectroscopic techniques) to elucidate a structure and its properties [14-19], may determine the reliability of the results, and may slow down decision-making during legal proceedings [20].

Considering the challenges regarding NPS, in silico methods [21,22] can be an alternative strategy to obtain information on these compounds. These methods rely on a wide range of software-based theoretical calculations, which provide information that can help to determine the properties of various compounds and systems [23,24]. These data can minimize errors and support more efficient analyses [25]. When validated through experimental data, in silico evaluation can be employed to acquire knowledge about a specific substance rapidly [26].

Here, we aimed to characterize Flakka [21,27-29] by theoretical methods. To fulfill our purpose, we carried out a Boltzmann distribution to pick up the minimum energy structure. Then, we employed a factorial design to obtain the best in silico conditions to reproduce the experimental data. Next, we used the best conditions to simulate spectral information. After that, we adapted a Python code to streamline spectrum extraction. Finally, we fitted theoretical results to the available experimental data. This procedure can provide directions to raise knowledge about NPS for which data are lacking, helping to improve information for forensic analysis [17,30].

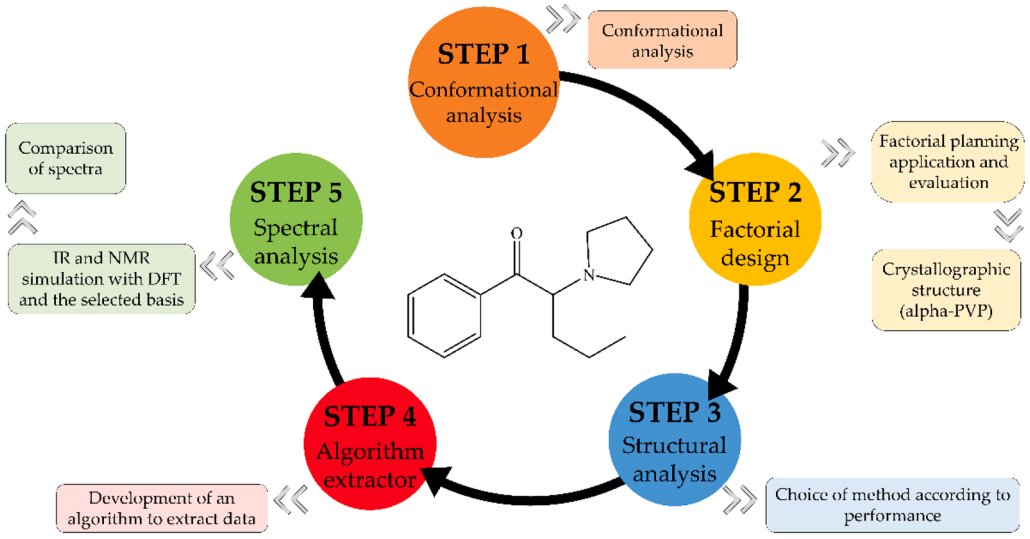

Fig. 1. Simplified scheme of the computational procedure.

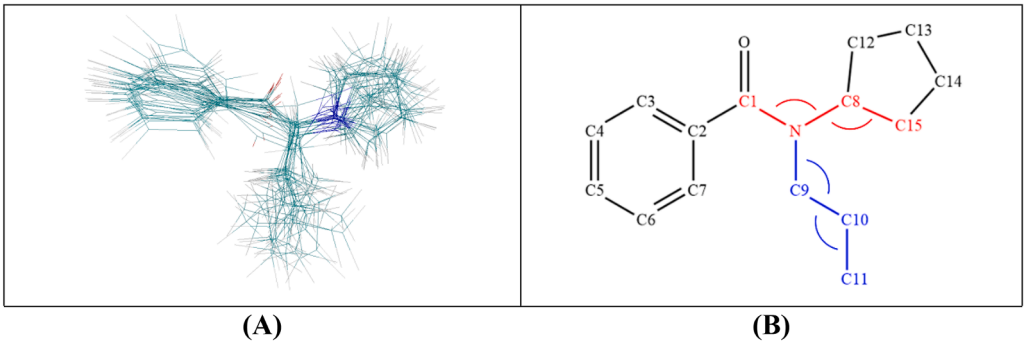

Fig. 2. Results for the Flakka structure: **(A)** overlapping of the optimized structures and **(B)** torsional angles with the respective evaluated dihedrals.

Table 3
Data referring to dihedral angles, RMSD, and Gibbs free energy for Flakka conformers.

Conformer	Gibbs free energy/ Eh	D(C1-C8-N-C15) /°	D(C8-C9-C10-C11)/°	RMSD
#01	−713.54181	74.00	−78.70	1.207
#02	−713.53961	−171.80	68.30	0.826
#03	−713.54626	68.10	73.30	1.140
#04	−713.53544	−46.20	92.60	1.099
#05	−713.54351	175.20	76.70	0.624
#06	−713.54341	67.60	172.10	0.976
#07	−713.54572	−62.30	61.00	1.302
#08	−713.54465	78.80	59.30	1.127
#09	−713.54527	−63.90	−77.60	1.141
#10	−713.54100	−174.80	−173.60	0.679
#11	−713.54512	66.70	−77.40	1.182
#12	−713.53520	−64.80	−70.10	0.975
#13	−713.54336	−176.20	−98.40	0.422
#14	−713.54132	70.20	−65.70	1.069
#15	−713.54675	−59.00	−72.60	1.151
#16	−713.54346	175.50	−61.60	0.689
#17	−713.54219	−79.30	−173.00	1.065
#18	−713.54023	−172.30	164.60	0.684
#19	−713.54735	66.50	−177.70	1.092
#20	−713.54538	179.00	−179.90	0.346
#21	−713.54323	71.00	−171.20	0.955
#22	−713.54474	174.60	−179.60	0.712
Reference	–	−173.40	−179.70	0

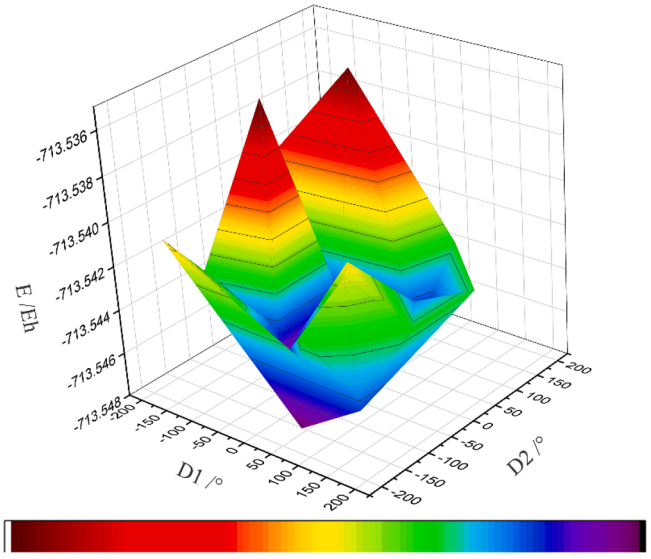

Fig. 3. 3D graphic representation of the conformational analysis for the Flakka structure: the × axis is the rotation increment of the D1 dihedral (C1-C8-N-C15); the y axis is the D2 dihedral (C8-C9-C10-C11), and the z axis is the Gibbs free energy values (E) for the structures.

Methods

STEP 1. Conformational analysis

Conformational analysis is essential to verify the possible structures and the conformational properties under study [31]. This procedure helps to understand global properties such as flexibility and to recognize possible conformers. There are some methods for this analysis, and Systematic Search is used in this work. This approach explores the conformational space through discrete variations of the twist angles with rotating connections [32,33]. The rotation values are predetermined so that a potential energy surface can be obtained. The dihedral increment of angle i (θ_i) is used to determine the number of conformations (S) relating to the number of free rotation angles (N) [34]. The number of possible conformers is given by Eq. (1):

$$S = \left(\frac{360}{\theta_i}\right)^N \tag{1}$$

However, depending on the structure, the number of conformations may increase exponentially due to rotational connections [35], which is the main disadvantage of this method. Optimizing geometry from X-ray structures is an alternative when there are many degrees of freedom. In some cases, the quality of conformational analysis is evaluated by comparing the calculated molecular geometries and the experimental data [36,37]. In the literature, there are examples presenting the coordinates taken from X-ray as the initial framework for optimization by the Density Functional Theory (DFT) [38-40]. We used the X-ray crystallographic coordinates as the starting input to perform conformational analysis.

Systematic conformational analysis was carried out by employing the Avogadro software [41] with the UFF force field [42]. The conformers were obtained by rotating dihedrals with free rotation, and the geometry was further optimized.

The obtained conformers were optimized by using the Orca software 4.1.0 [43], and a theoretical level of DFT[44] B3LYP [45,46]/6-31G** was applied [47]. The absence of imaginary values in the vibrational calculation modes indicates a minimum of true energy [48,49]. These results for Gibbs free energy, dihedral angle values, and RMSD (Root Mean Square Difference) were evaluated [50]. RMSD was used to calculate the distances between the conformations obtained after optimizations with the crystallographic structure. RMSD provides a measure of the average distance between the atoms of two or more molecules, according to Eq. (2):

$$RMSD = \frac{1}{N}\sqrt{\sum_{i=1}^{N_{atoms}} \left(r_i(t_1) - r_i(t_2)\right)^2} \tag{2}$$

The Gibbs free energy values were also used to perform the Boltzmann Distribution (p_i). This approach allows the probability that conformers (i) occur in solution at a given temperature (T) to be evaluated. The diversity of conformers at equilibrium at 298.15 K can be measured by Eq. (3) [51],

$$p_i = \frac{\exp\left(-\frac{E_i}{k_B T}\right)}{\sum_{j=1}^{N} \exp\left(-\frac{E_i}{k_B T}\right)} \tag{3}$$

where k_B is a Boltzmann constant (0.001987 kcal mol^{-1} K^{-1}), N is the number of conformers, and E_i is the electronic energy of conformer i in the ground state. All the selected values are normalized.

STEP 2. Factorial design

Factorial Design reduces the number of experiments, thereby decreasing operational costs and time and minimizing variation in data processing [52-56]. This type of planning uses two concepts: factors and levels. Factors are independent variables submitted to pre-determined variations in the experimental conditions; these variations are called levels. A factorial design with two levels is best represented by using (+) for the high level and (-) for the low level. The planning results provide a combination of all the factors at all the levels, to determine how the variables affect the procedure [55,56].

To evaluate the spectroscopic properties of a molecule, conditions for quantum chemistry calculations are significant. Knowing the best combination is necessary to obtain adequate results. Here, the results were systematically evaluated by factorial planning. A 2^3 factorial design (two levels and three factors) was conducted; the factors were DFT, Basis-set, and Correction. Regarding DFT, B3LYP was used: it is the most employed in research because it has empirical parameters and is a

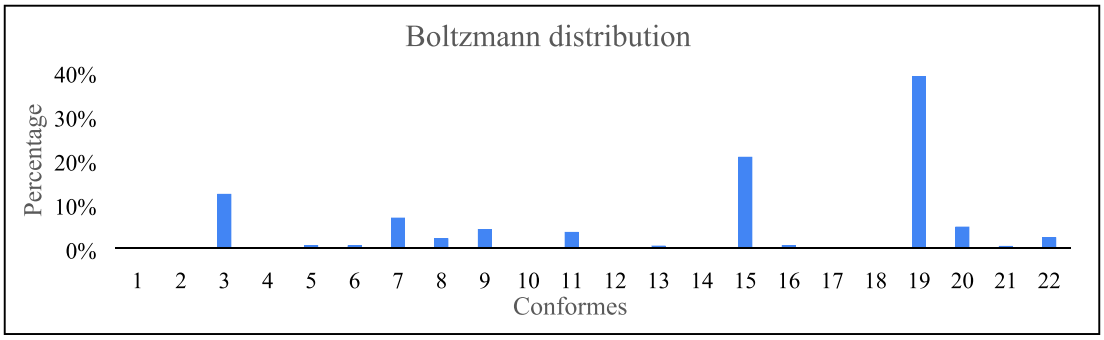

Fig. 4. Graphic representation of the percentage relative to the Boltzmann distribution for the possible structural conformations of Flakka.

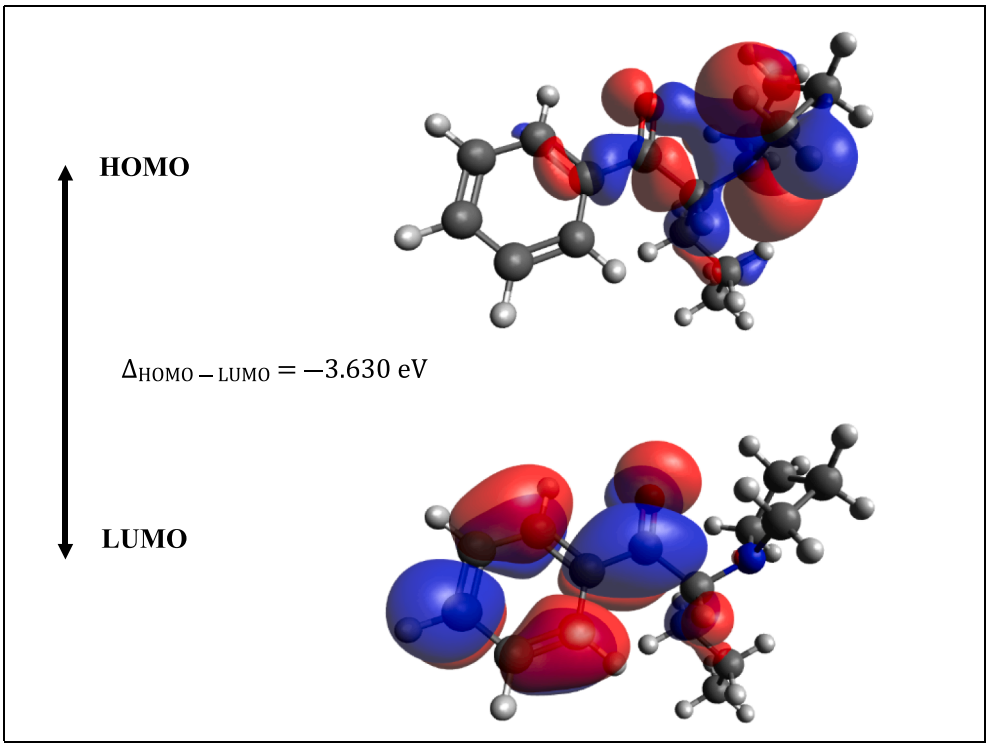

Fig. 5. Representation of the HOMO and LUMO orbitals of the Flakka molecule and the respective energy gap value ($\Delta_{HOMO-LUMO}$).

Table 4
Energy gap between the HOMO and LUMO orbitals for Flakka structure #19.

	E/Eh	E/eV
HOMO + 3	−0.2576	−7.0096
HOMO + 2	−0.2545	−6.9249
HOMO + 1	−0.2487	−6.7685
HOMO	−0.1860	−5.0613
LUMO	−0.0526	−1.4313
LUMO-1	−0.0069	−0.1886
LUMO-2	0.0427	1.1620
LUMO-3	0.0814	2.2145

Table 5
Results related to experimental design.

Experiment	Computational time/minutes	RMSD
1	555.85	0.223
2	567.25	0.259
3	330.71	0.258
4	311.23	0.266
5	493.16	0.268
6	549.31	0.277
7	324.40	0.307
8	299.90	0.291

hybrid model with non-local approximation [57,58]. PBE0 was selected because its parameters are only based on fundamental constants, and it has a semi-local approach [57,58]. The Basis-set levels were TZVP and 6-31G **. They were selected because they can describe all the atoms present in the system under study and are widely employed for theoretical spectroscopic and NMR calculations. Another reason for choosing DFTs was that their scaling factors were determined in the same work [59]. The third factor, the D3BJ dispersion correction proposed by Grimme and coworkers, is largely used [60,61]. Precise evaluation of these corrections is essential when studying intermolecular interactions of organic molecules [62] because it can provide elements that can describe a more improved geometry, significantly influencing the quality of the responses. These factors are the most important when the influence on the calculation time and quality of the final geometry is evaluated. Given that three factors were varied herein, complete planning was selected because it provides a broad view of the responses that

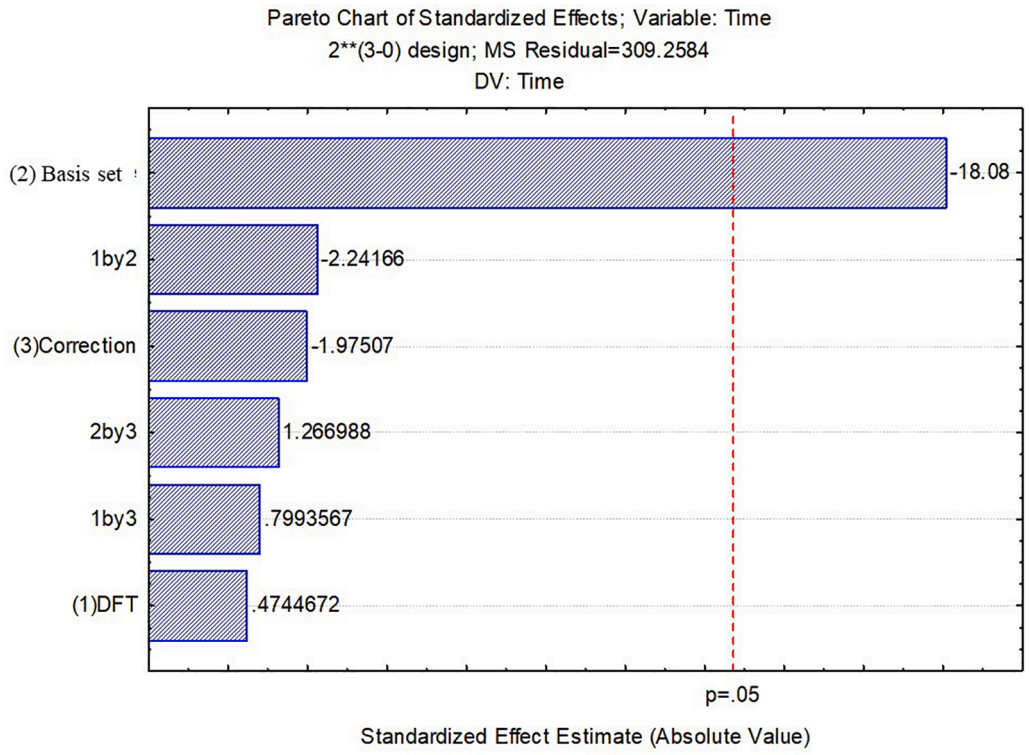

Fig. 6. Pareto Chart for Computational Time.

are being evaluated. The use of this planning proved to be adequate because the number of factors was well delimited.

These conditions represent qualitative levels, which were selected according to literature information [63]. These parameters were selected for the present study. In systems with different atoms or dimensions, other parameters could be preferred. The number of factors can be selected depending on the response someone is interested in. Many calculation conditions can be addressed, but this would significantly increase the number of experiments. In this case, fractional factorial design could be used. Furthermore, factorials with a central point and axial points exist. However, these plans require quantitative factors. DFT-based simulation methods do not allow these factors to be fractionated or the exact fraction to be used as a central or axial point in the factorial design to be determined. For these reasons, the complete experimental design proved the best alternative.

Although many DFT and basis-set options can be used for this purpose, here factorial planning was used for rational choice of the best DFT/basis-set combination to describe our system. This planning can provide a tool to evaluate the responses for the combinations. To validate the results, experimental responses were employed in the comparison.

Tables 1 and 2 show the factorial design:

The planning was performed with the starting structure based on the crystallographic structure of the target drug, available in The Cambridge Crystallographic Data Center platform [64]. Table 2 lists the data and indicates the factors and levels used in each experiment. The results were obtained by employing the Orca software [43]. All the details for the numerical precision are in the Supporting Information Section.

From the data generated (output) by performing the procedure proposed in part 1, the influence of each factor was evaluated by using the Statistica software [65]. Analysis of variance (ANOVA) was carried out, to obtain Contour graphs and Pareto Chart with 95% confidence interval, which showed which factors were significant for the analysis of the results. The results were compared for all the combinations to obtain the best conditions for the calculation. RMSD [50] (Eq. (2)) and calculation time values were compared.

STEP 2.1 structural analysis of factorial design experiments

Besides the data obtained in the first step, the structure was evaluated by comparing bond lengths and bond angles with the experimental values of the crystallographic structure. The Avogadro software was employed. In this way, the method that best corresponded to the target substance was defined and applied in later calculations. The X-ray crystallographic coordinates were used as the starting input coordinates for the DFT calculations. The crystalline structure was employed as a parameter to indicate the minimum energy [66,67]. Many papers present the coordinates taken from X-ray as the initial framework for optimization by DFT [36-40]. The calculated molecular geometries are usually compared with the X-ray data, and agreement between them is checked [68,69].

After optimization, the geometric parameters (bond lengths, bond angles, torsion angles) for the compound were compared with the experimental data. In addition to the structural comparison, the absence of imaginary values in the vibrational calculation modes indicates a minimum of true energy [48,49]. The calculated vibrational modes and the predicted ^{1}H and ^{13}C NMR chemical shifts were scaled to the same level of theory.

STEP 3. Adaptation of algorithm for extracting and manipulating data

An algorithm in Python programming language [70-73] was developed by using the Repl.it web platform [74] to develop the script. This made extraction of the data obtained in the frequency calculations automatic, thus avoiding possible errors and optimizing the execution time. Concerning script elaboration, the idea was to find a pattern of words/syntaxes that allowed the desired information to be extracted from the defined pattern and stored in a new text file. The Repl.it environment was selected because it is a free web platform that enables scripts to be developed in different programming languages,

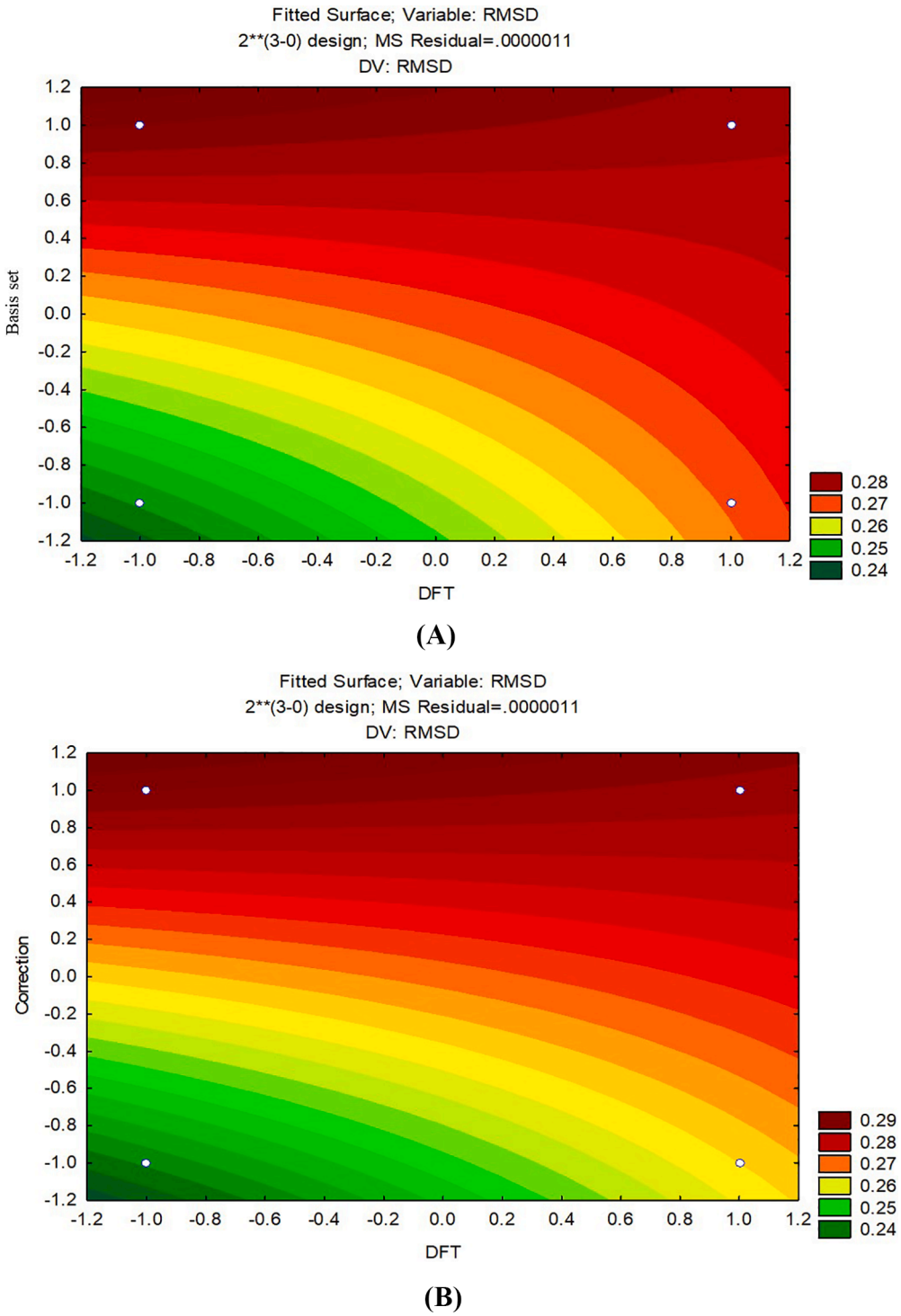

Fig. 7. **(A)** DFT × Basis-set Contour graph for RMSD; **(B)** DFT × Correction Contour graph for RMSD; **(C)** Pareto Chart for RMSD.

individually or in shared online rooms, thereby ensuring total accessibility to any user that has an internet connection.

STEP 4. Comparison of theoretical and experimental spectra by multivariate methods

The frequency and chemical shifts were calculated by using the Orca v.4.1.0 software [43]. On the basis of the results of the previous steps, the method that provided the best performance was employed. The positive numerical result of the frequency values confirmed that the structure was in a minimum state of energy, which allowed the Infrared spectrum to be simulated and compared with the experimental spectrum described in the literature.

The theoretical Infrared spectrum between 400 and 4000 cm^{-1} was simulated. Because the theoretical spectra use harmonic approximations and do not consider some anharmonic effects in the calculations, the energy values were higher compared with the experimental results [75,76]. To correct these responses, a scale factor that had already been

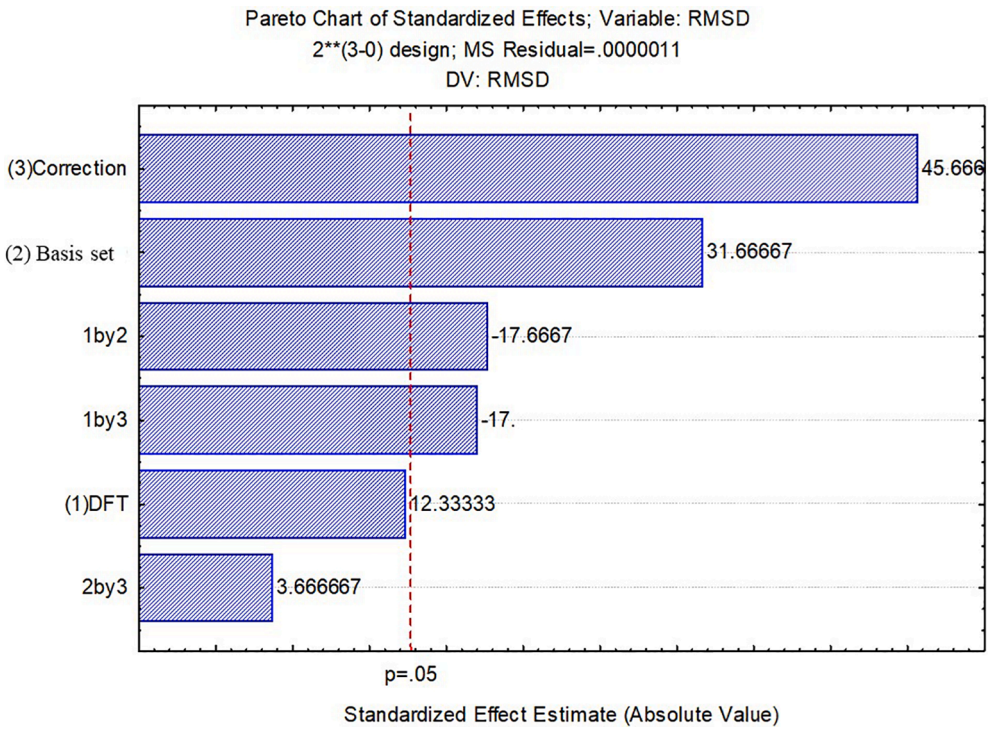

Fig. 7. (*continued*).

Table 6
Comparison between α-PVP bond length and bond angles.

Bond Length/A°									
	1	2	3	4	5	6	7	8	Exp.
C4-C5	1.394	1.390	1.398	1.394	1.394	1.390	1.399	1.395	1.391
C3-C4	1.385	1.382	1.390	1.387	1.386	1.383	1.391	1.387	1.384
C2-C3	1.401	1.397	1.405	1.401	1.402	1.398	1.407	1.402	1.396
C2-C7	1.400	1.396	1.404	1.400	1.401	1.397	1.406	1.401	1.398
C7-C6	1.389	1.386	1.394	1.390	1.390	1.386	1.395	1.391	1.388
C6-C5	1.391	1.388	1.396	1.393	1.392	1.388	1.397	1.393	1.382
C12-C13	1.533	1.526	1.537	1.530	1.535	1.527	1.538	1.531	1.524
N-C12	1.520	1.506	1.522	1.509	1.525	1.508	1.527	1.512	1.524
C13-C14	1.532	1.523	1.534	1.526	1.533	1.524	1.535	1.526	1.522
C14-C15	1.520	1.513	1.524	1.517	1.522	1.514	1.526	1.518	1.515
C15-N	1.503	1.489	1.503	1.489	1.508	1.491	1.507	1.491	1.511
N-C8	1.489	1.477	1.491	1.480	1.498	1.481	1.499	1.483	1.500
C11-C10	1.530	1.523	1.534	1.527	1.533	1.524	1.537	1.528	1.522
C1-O	1.212	1.208	1.219	1.215	1.212	1.208	1.220	1.215	1.219
C9-C10	1.529	1.521	1.534	1.526	1.532	1.523	1.537	1.527	1.526
Bond Angle/°									
C8-N-C15	113.7	113.6	113.7	113.7	113.6	113.5	113.5	113.6	113.5
C2-C1-C8	118.5	118.4	118.7	118.9	119.0	118.7	119.2	119.2	117.8
C9-C10-C11	111.1	111.0	111.3	111.4	111.2	111.1	111.5	111.5	111.4
C12-C13-C14	104.1	103.8	104.0	103.8	104.3	103.8	104.2	103.8	104.2
C2-C3-C4	120.5	120.4	120.5	120.4	120.6	120.5	120.6	120.5	120.2
O-C1-C8	120.1	120.1	119.8	119.8	120.0	120.1	119.6	119.7	119.9
C8-N-C12	114.6	114.4	114.9	114.8	114.7	114.5	115.0	114.8	113.8
C12-N-C15	107.2	107.3	107.3	107.3	106.9	107.2	107.0	107.2	106.5
C3-C2-C7	119.1	119.2	119.3	119.4	118.9	119.1	119.1	119.3	119.7

calculated and which is available from the National Institute of Standards and Technology was used [77]. This factor is calculated for each DFT/Basis-Set combination. For this work, the scaling factors 0.9608 (B3LYP/6-31G**), 0.9654 (B3LYP/TZVP), 0.9863 (PBE0/6-31G**), and 0.9888 (PBE0/TZVP) were employed.

The chemical shift values were obtained by using tetramethylsilane (TMS) as reference, which is the most common reference in this type of analysis. By employing the same method selected in the factorial design, the average ^{13}C and ^{1}H shifts for TMS (192.76 ppm and 31.7065 ppm, respectively) were calculated and subtracted from the values obtained for the study molecule. All the carbons or hydrogens were considered because the structure is symmetric, and the displacements are identical. Moreover, a simple average was performed for these values. In this step, the responses obtained previously were used and recalculated for the parameters that had already been optimized: the structure of Flakka with chloroform. For this purpose, CPCM implicit solvent (conductor-like polarizable continuum model) was employed [78,79]. Chloroform ($CDCl_3$) was the CPCM implicit solvent [78,79], and the theoretical

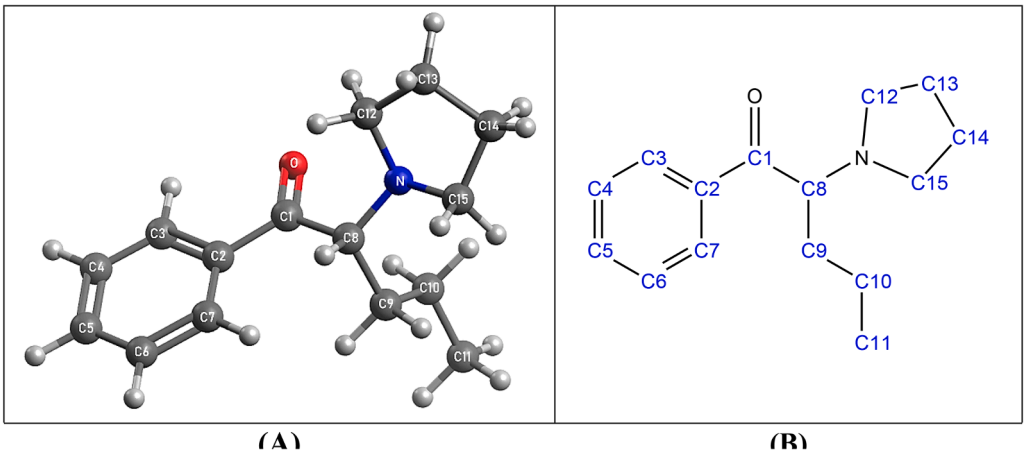

Fig. 8. Structural representation and indication of the numbering of atoms in **(A)** 3D and **(B)** 2D.

Table 7
Coefficients of Determination (R^2) for bond length and bond angle.

Factorial Experiment (FacExp)	R^2 – Bond length	R^2 – Bond angle
1	0.9951	0.9932
2	0.9899	0.9932
3	0.9938	0.9913
4	0.9885	0.9907
5	0.9971	0.9899
6	0.9915	0.9918
7	0.9961	0.9870
8	0.9901	0.9883

Table 8
Categories of analytical techniques according to SWGDRUG [8].

Category A	Infrared Spectroscopy, Mass Spectrometry, NMR Spectroscopy, Raman Spectroscopy, X-Ray Diffractometry.
Category B	Capillary electrophoresis, gas chromatography, liquid chromatography, supercritical fluid chromatography, thin layer chromatography, ion mobility spectrometry, microcrystalline tests, UV–Visible spectroscopy.
Category C	Colorimetric tests, fluorescence spectroscopy, immunoassay, melting point, pharmaceutical identifiers.

results were compared with the experimental data [80]. The calculations involving NMR were carried out for the molecule with HCl and for the free-base molecule.

The study was divided into four steps as described below and schematically represented in Fig. 1.

Results and discussion

STEP 1. Conformational analysis

With the aid of the Avogadro software, we obtained the 26 conformers of the Flakka structure, with a 13.8° angle increment. We optimized a total of 26 conformers with DFT B3LYP/6-31G**, and 22 of them returned viable optimizations. We compared the optimized responses to the crystallographic structure in terms of the RMSD parameter (Fig. 2**A**) and dihedral angles (Fig. 2**B**). The data referring to the dihedral angles, RMSD, and Gibbs free energy are grouped in Table 3.

We entered the energy and dihedral angle data into the Origin 2020 software to help us to read the information. Fig. 3 schematically shows the results obtained for the energies compared to the respective dihedral angles. The region where the energy was minimal is formed by conformers #19 (-713.54735 Eh), #15 (-713.54675 Eh), and #03 (-713.54626 Eh).

When we analyzed the results by RMSD, these minimum energy structures were at most around 1 Ã… away from the crystallographic structure. The values ranged from 0.346 for conformer #20 to 1.302 for conformer #07; the conformers with lower energy diverged by 1.092 (#19), 1.140 (#03), and 1.151 (#15). Therefore, we performed the Boltzmann distribution analysis by using the Gibbs free energy as a parameter. This assessment allowed us to determine the probability of observing each conformer, and we obtained the graph represented in Fig. 4.

The most abundant conformers were #19 (39.08%), #15 (20.74%), and #03 (12.32%). The sum of the percentages of the other conformers was 27.89%. On the basis of these results, we used the structure of the #19 input conformer for the next steps.

On the basis of structure #19, we evaluated the energy gap between the frontier orbitals (Fig. 5), the highest occupied molecular orbital energy (E_{HOMO}), and the lowest unoccupied molecular orbital energy (E_{LUMO}), and their respective variations from HOMO + 3 to LUMO-3. Through these values, we can understand properties such as the ability of a molecule to supply electrons (E_{HOMO}) or the ability of a compound to accept electrons (E_{LUMO}) [81,82]. These values can provide important information about the stability and reactivity of molecules and are represented in Table 4.

The HOMO-LUMO energy gap helps us to understand the electronegativity (χ) of the analyzed structure. Electronegativity can be expressed by Eq. (4) [83].

$$\chi = \frac{-(E_{HOMO} + E_{LUMO})}{2} \quad (4)$$

The greater the difference between the $E_{HOMO\text{-}LUMO}$ orbitals, the lower the chemical reactivity, and the greater the kinetic stability. In this case, the electronegativity value was 3.2463 eV. This information is important to understand chemical interactions (separation methods for example) [84,85] and possible biological effects [86].

STEP 2. Factorial design

We analyzed the results concerning the performance of each experiment on the basis of two parameters: computational time and RMSD. Table 5 groups the results obtained by simulation for the eight experiments outlined in the experimental design.

We applied the values of the responses obtained from the experiments and the coded matrix of the experiments to analyze the information. By using the Statistica 7 software [65], we established the best approach among the approaches delimited in the experimental planning. Figs. 6 and 7 display the results for the Pareto Chart with 95% confidence interval.

The Contour graph results (Fig. 7**a and b**) helped us to visualize how

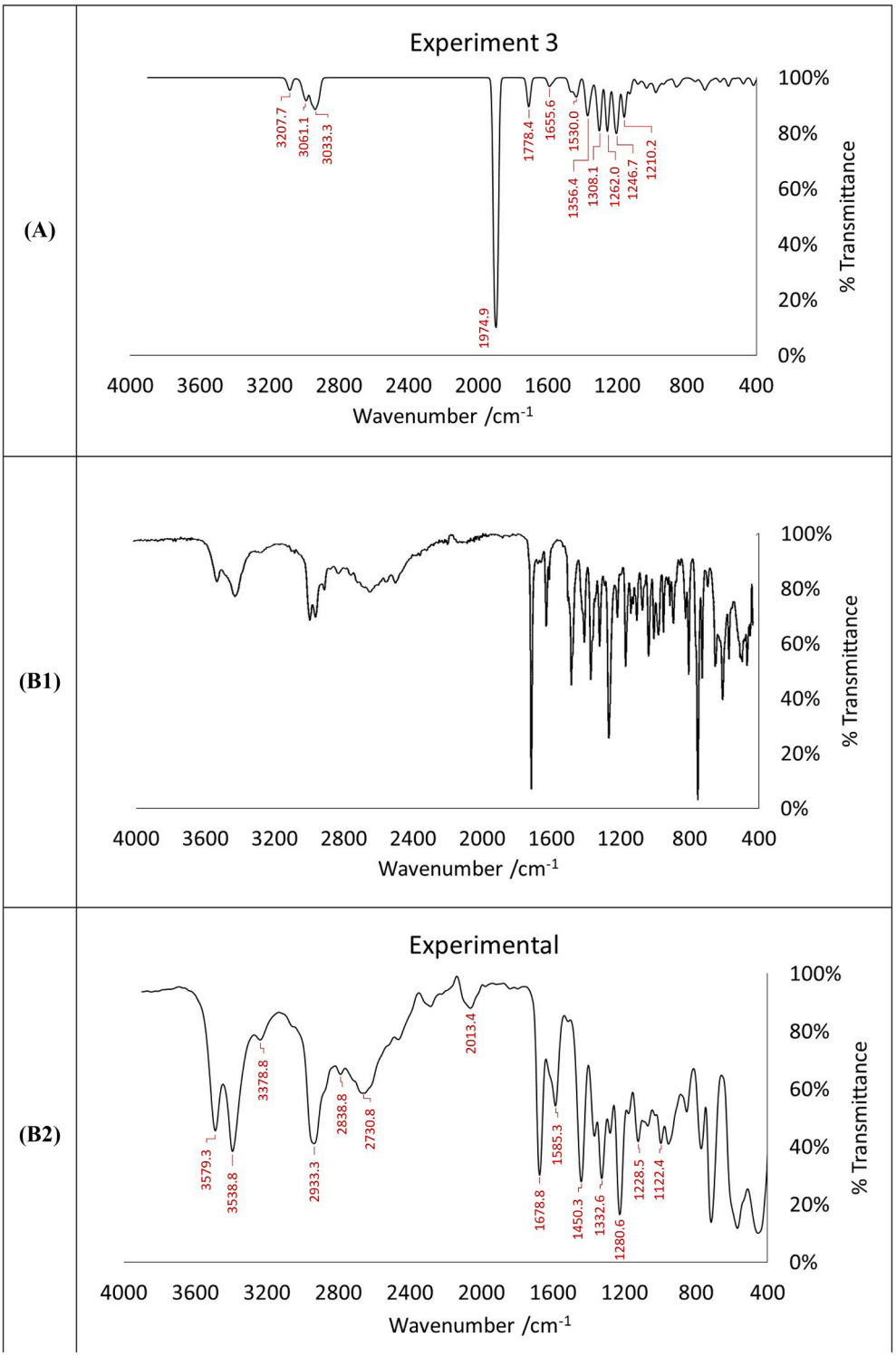

Fig. 9. **(A)** Theoretical Infrared Spectrum of α-PVP. **(B)** Experimental infrared spectrum of α-PVP **(B1)** 81 and **(B2)** [92].

the parameters evaluated by the experimental design influenced the responses. These graphs correspond to response gradients, wherein red and green refer to the parameters that resulted in the lowest and largest responses, respectively. Thus, the responses of the TZVP database presented the highest computational time values and the lowest RMSD. Regarding the DFTs, the contour graph revealed a difference in the visual response. However, on the basis of the technical needs of forensic chemistry, we selected DFT B3LYP. The Pareto graph (Fig. 7**c**) helped us to understand and to observe the significance of each of the analyzed parameters and how one influenced the other. This type of response can assist in a more adequate and objective choice of parameters for quantum calculations. Thus, we statistically understood that, depending on the applied type of basis-set, the computational time and RMSD parameters greatly influenced the results obtained without many calculations with various DFT and bases being performed.

The use of contracted functions, such as the split-valence double-zeta plus polarization basis-set Pople's 6-31G**, reduces the computational cost because the number of optimized parameters becomes smaller

Table 9
Reference values used to compare the theoretical and experimental spectra [93].

B1	C–H (aromatics – out-of-plane bend)	900–690
B2	C-N (amines)	1350 – 1000
B3	$–CH_3$ (bend)	1450 – 1375
B4	$–CH_2$- (bend)	1465
B5	N–H (primary and secondary amines bend)	1640 – 1550
B6	C = O (ketone)	1725 – 1705
B7	C–H (stretch)	3000 – 2850
B8	Aromatics (stretch)	3150–3050
B9	N–H (primary and secondary amines stretch)	3500 – 3100

Table 10
Comparison between the bands referring to the theoretical and experimental spectra, according to the reference values.

	B1	B2	B3	B4	B5	B6	B7	B8	B9
Experimental	1	1	1	1	1	1	1	1	1
Theoretical	0	1	1	1	1	1	1	1	1

without the precision of the method being lost [87-91].

The triple-zeta valence function Alrich's TZVP with polarization uses one contracted Gaussian function to describe the inner shells and three Gaussian functions to describe de valence shells. Because it is a more extensive basis-set, the computational cost is higher compared to 6-31G** [90,91].

A factor that contributes to the accuracy of the results is the size of the basis-set, as well as the different types of functions that the set presents. Therefore, the best RMSD results obtained by using the TZVP basis-set is justified. Notwithstanding, the basis-set 6-31G** provided satisfactory results if we consider the low complexity of the molecule.

Regarding computational time, using 6-31G** optimized the results because this basis-set has reduced computational processing cost, affording better responses compared to TZVP. Along with the analytical evaluation, this aspect must be considered in the forensic context when we select the method: fast processing of the results related to drugs is becoming increasingly urgent due to the need to keep up with the emergence of new substances.

STEP 2.1 structural analysis of factorial design experiments

We used the data obtained from the experiments to compare the crystallographic structure of α-PVP with the structure obtained for this substance by the computer simulation indicated in the planning (Table 6). We numbered the atoms as shown in Fig. 8.

We carried out the structural evaluation by correlating the values of bond length and bond angle obtained from each theoretical experiment with the experimental values in linear regression graphs, which can be seen in Supporting Information. Table 7 lists the coefficients of determination (R^2).

In general, all the methods showed good correlation with the original structure. Among them, experiments 1 (B3LYP/TZVP/D3BJ) and 3 (B3LYP/6-31G**/D3BJ) stood out: the R^2 values were close to 1 for both bond length and bond angle.

Experiments 4 (PBE0/6-31G**/D3BJ) and 8 (PBE0/6-31G**/-) gave the least satisfactory results in terms of structural comparison. If we consider the results obtained in the planning and structural evaluation stages, B3LYP/6-31G**/D3BJ (Experiment 3) was the most efficient method for forensic needs. Therefore, hereafter all the discussions will be based on the results of the method proposed by Experiment 3.

Table 11
Correlation between simulated and experimental spectra.

	R^2	Equation	$\lambda_{Error(max)}$	$\%Error_{max}$	$\lambda_{Error(min)}$	$\%Error_{min}$	*SD*
Exp. 1	1.0000	1.0000x – 0.7447	624.85	1.61	3122.29	0.00	0.0029
Exp. 2	1.0000	1.0002x – 0.7893	590.14	1.51	838.92/1189.91/3041.30	0.01	0.0039
Exp. 3	1.0000	0.9993x – 1.1881	692.35	1.53	678.85/3216.79	0.00	0.0032
Exp. 4	1.0000	1.0001x – 1.7910	771.42	2.05	1398.20/1504.25	0.00	0.0046
Exp. 5	1.0000	1.0024x – 6.0384	773.91	1.46	3054.80	0.00	0.0037
Exp. 6	1.0000	1.0003x – 1.5281	590.14	1.60	1797.42/3054.80	0.00	0.0038
Exp. 7	1.0000	0.9996x – 1.0963	497.57	1.65	1531.27/1967.13	0.00	0.0036
Exp. 8	1.0000	1.0002x – 0.7796	692.35	1.98	439.71/1108.91/3162.79	0.00	0.0042

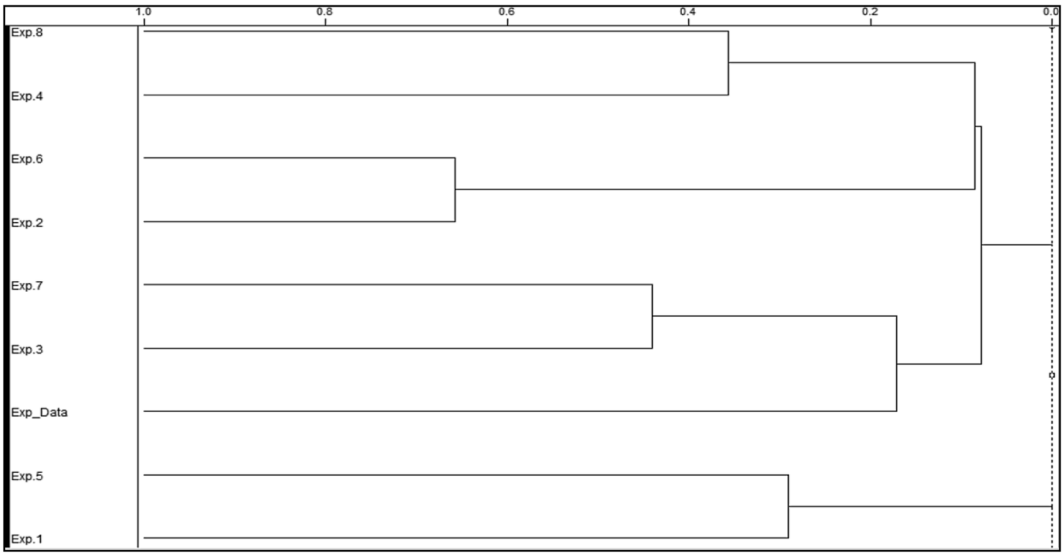

Fig. 10. HCA results for spectral comparison.

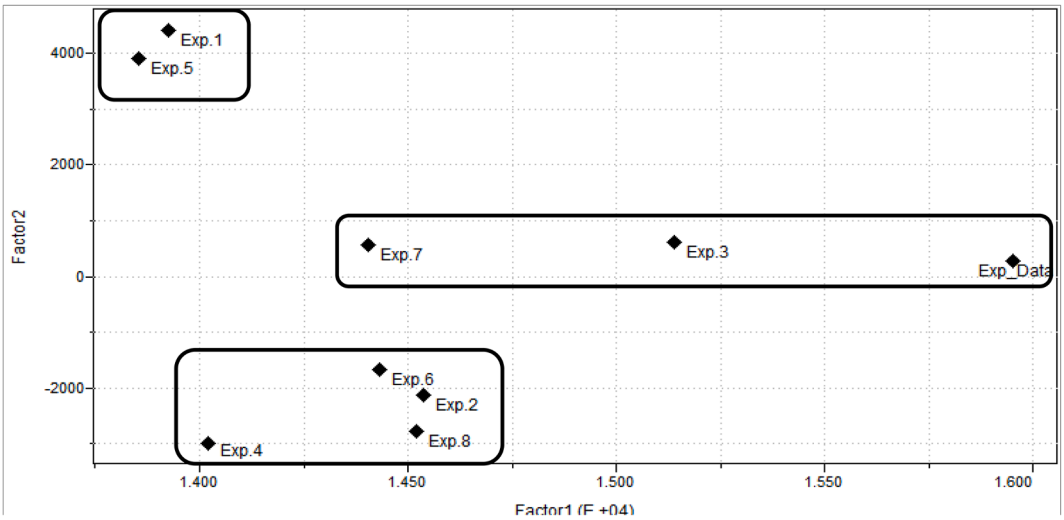

Fig. 11. PCA results, which showed that similar experiments are along Factor2.

Table 12
Univariate statistical analysis of the wavelengths of the spectra obtained by simulation as compared to the experimental one.

Factorial Experiment	KL for original data	KL for the average spectral line intensities in intervals of 4 cm^{-1}
Exp. 1	0.0503	0.1795
Exp. 2	1.8964	1.9379
Exp. 3	0.0811	0.2239
Exp. 4	0.0944	0.2052
Exp. 5	0.0217	0.0834
Exp. 6	0.0634	0.1448
Exp. 7	2.0462	2.1843
Exp. 8	0.0819	0.2137

Table 13
Comparison between theoretical and experimental results of carbon chemical shifts for α-PVP HCl.

Atom numbering	Theoretical/ppm	Experimental/ppm	$\lvert\Delta(Exp. - Theo.)\rvert$
C1	194.9	196.7	1.8
C2	134.7	135.7	1.0
C3	129.0	128.6	0.4
C4	128.2	129.4	1.2
C5	127.4	129.4	2.0
C6	131.0	135.1	4.1
C7	128.3	128.6	0.3
C8	76.2	62.7	13.5
C9	36.5	33.0	3.5
C10	20.3	19.6	0.7
C11	16.7	14.0	2.7
C12	58.8	49.4	9.4
C13	27.9	23.7	4.2
C14	28.8	24.0	4.8
C15	56.0	52.9	3.1

STEP 3. Adaptation of algorithm for extracting and manipulating data

To understand the script better, we numbered the lines and laid out their interpretation in Supporting Information. If we consider the difficulties inherent in manipulating the large data sets generated during these types of analysis, application of this script significantly reduced the data processing time and minimized the spread of possible random errors.

Table 14
Comparison between theoretical and experimental results of hydrogen chemical shifts for α-PVP HCl.

Atom numbering	Theoretical/ppm	Experimental/ppm	$\lvert\Delta(Exp. - Theo.)\rvert$
H1	11.96	12.48	0.52
H2	8.50	7.99	0.51
H3	7.81	7.56	0.25
H4	7.89	7.70	0.19
H5	7.70	7.56	0.14
H6	8.08	7.99	0.09
H7	4.62	5.26	0.64
H8	1.94	2.04	0.10
H9	2.16	2.20	0.04
H10	0.86	1.36	0.50
H11	1.88	1.48	0.40
H12	0.73	0.91	0.18
H13	1.07	0.91	0.16
H14	0.61	0.91	0.30
H15	2.50	3.62	1.12
H16	3.96	3.82	0.14
H17	2.01	2.20	0.19
H18	1.90	2.20	0.30
H19	2.67	2.04	0.63
H20	2.57	2.20	0.37
H21	2.79	2.93	0.14
H22	3.65	3.82	0.17

Table 15
Comparison between theoretical and experimental results of carbon chemical shifts for α-PVP (free-base).

Atom numbering	Theoretical/ppm	Experimental/ppm	$\lvert\Delta(Exp. - Theo.)\rvert$
C1	210.75	201.20	9.55
C2	144.83	137.10	7.73
C3	140.28	128.60	11.68
C4	137.81	128.40	9.41
C5	135.24	132.90	2.34
C6	134.86	128.40	6.46
C7	134.13	128.60	5.53
C8	74.48	68.80	5.68
C9	33.97	32.80	1.17
C10	29.65	19.30	10.35
C11	16.22	14.30	1.92
C12	61.15	51.00	10.15
C13	28.63	23.40	5.23
C14	24.91	23.40	1.51
C15	50.08	51.00	0.92

Table 16
Comparison between theoretical and experimental results of hydrogen chemical shifts for α-PVP (free-base).

Atom numbering	Theoretical/ppm	Experimental/ppm	$\lvert\Delta(Exp. - Theo.)\rvert$
H1	8.62	8.12	0.50
H2	7.73	7.45	0.28
H3	7.87	7.55	0.32
H4	7.78	7.45	0.33
H5	8.36	8.12	0.24
H6	4.16	3.91	0.25
H7	1.81	1.91	0.10
H8	1.67	1.75	0.08
H9	1.68	1.23	0.45
H10	1.62	1.29	0.33
H11	0.92	0.87	0.05
H12	0.88	0.87	0.01
H13	0.77	0.87	0.10
H14	2.54	2.58	0.04
H15	2.12	2.58	0.46
H16	1.16	1.91	0.75
H17	1.10	1.75	0.65
H18	1.06	1.75	0.69
H19	3.02	1.91	1.11
H20	3.25	2.68	0.57
H21	3.21	2.58	0.63

STEP 4. Theoretical compared to experimental spectra using multivariate methods

On the basis of factorial design, we have already been able to evaluate the performance of in silico methods and their influence in generating a response that is in line with the experimentally observed one. From this, we rely on two techniques classified as the gold standard of confidence for substance identification, as indicated by SWGDRUG [8]. The techniques performed here belong to category A. Table 8 presents these techniques, and others, according to their categories.

STEP 4.1 infrared spectra

Fig. 9 compares the experimental and the theoretical spectra that best corresponded to the previous steps. The spectral simulation of the other theoretical experiments can be found in Supporting Information.

We compared the theoretical results with the experimental results from a binary table, where "1″ represents presence of the band, and "0″ represents absence of the band. Table 9 summarizes the values that we used as reference to attribute the bands; Table 10 compares the bands, indicating their presence or absence.

Comparison between the infrared bands of the theoretical and experimental spectra revealed good correspondence, validating the proposed method. Due to the high stretch intensity in the 1974.93 cm^{-1} region, probably chlorine, the other peaks were covered up. Therefore, we removed this band, to allow the spectrum to be visualized.

We also compared the calculated spectra with the experimental one [92]. We compared all the spectra calculated from the experiments generated in factorial planning. To evaluate the agreement between the responses of the spectra, we performed three different procedures. In the first one, we analyzed the linear correlation (R^2) of the spectroscopy data in the infrared region. The closer to 1, the greater the similarity. Table 11 presents the results. The equation of a line is presented in the third column. The fourth and fifth columns show the wavelengths with the highest percentage of error. Similarly, the sixth and seventh columns show the wavelengths with the lowest percentage. The last column corresponds to the standard deviation (SD) obtained from each equation of a line.

Results from Table 11 showed a high linear correlation between all the simulated and experimental data. The greater percentage of errors occurred in the fingerprint region, between 400 and 900 cm^{-1}. The other regions showed a low percentage error (>1%). As for the percentage errors, standard deviations were small in all cases. Analysis of these responses followed the planning we carried out, indicating DFT B3LYP with D3BJ dispersion correction as they better reproduced the experimental data in this study. Concerning the employed basis, they practically did not differ. However, in a forensic context where the speed of responses is an important factor, the basis 6-31G ** showed greater performance.

We also compared the spectra through multivariate unsupervised analyses. Hierarchical Cluster Analysis (HCA) and Principal Component Analysis (PCA) are used to explore multivariate data. We used them to analyze the clustering regarding the calculation responses. HCA allows us to assess how similar the experiments are through the distances between them. PCA consists in a transformation of multivariate data to a new coordinate system by means of linear combination of the original variables. It is a technique that evaluates the natural organization with no influence of previous information about the system. Both methods allow data in smaller dimension to be visualized, which facilitates observation of similarities among the samples [94-96].

For HCA, we used the Euclidean Distance and the Single linkage method [94]. No preprocessing was used. The dendrogram indicated in Fig. 10 showed the higher approximation between the experimental data and the data from experiments that used B3LYP as DFT.

Fig. 10 shows the results for clustering of the different experiments. We observed that Experiments 1 (B3LYP/TZVP/D3BJ) and 5 (B3LYP/TZVP/-) had the most significant divergence from the others. Experiments that used PBE0 as the DFT also grouped together (Experiments 2, 4, 6 and 8), and we observed the influence of the basis-set on the clustering. B3LYP/6-31G** (Exp. 3) was the combination with the most significant similarity with the experimental data obtained from the literature [92]. These responses confirmed the conclusions obtained from the factorial design. The PCA results are presented in Fig. 11. The cumulative variance in two principal components (factor 01 and factor 02) was around 94%. The results resembled the HCA results, showing that Exp. 03 was the closest to the experimental data.

In addition to the similarity with Exp. 3, PCA enabled us to visualize the formation of three groups. One of them consisted of experiments in which DFT PBE0 (the even-numbered experiments) was used; the other two were created by DFT B3LYP. One was grouped by the TZVP basis (Exp.1 and Exp.5); the other was grouped by the 6-31G** basis (Exp.7 and Exp.3).

We also used the Kullback–Leibler (KL) Divergence to compare the spectra [97,98]. In this methodology, each pair of spectra P and Q is compared by

$$D_{KL}(P,Q) = \frac{[D_{KL}(P||Q) + D_{KL}(Q||P)]}{2} \tag{5}$$

where

$$D_{KL}(P||Q) = \sum_i P(i) log \frac{P(i)}{Q(i)} \tag{6}$$

and P and Q are the normalized IR spectra.When there is no difference between the spectra, $D_{KL} = 0$.

Table 12 presents the KL divergence results. We calculated the distances between the simulated and experimental spectra. For each comparison, we took the original results and the average of spectral line intensities in intervals of 4 cm^{-1}. We removed the signal corresponding to the hydrochloride form from the experimental spectra.

KL divergence results showed that most spectra simulated with B3LYP provided the closest results to the experimental data (Exp. 1, Exp. 3, Exp. 5). Although Exp. 7 used the B3LYP/6-31G** combination, the D3BJ correction was absent. These results emphasized the importance of applying the correction.

STEP 4.2 nuclear magnetic resonance

The NMR results we obtained by using the parameters defined by Experiment 3 (B3LYP/6-31G ** combination) are based on published

works [99-104]. Double zetta bases are adequate for obtaining carbon and hydrogen chemical shifts without the theoretical rigor and computational cost of larger bases being necessary [105].

We assigned the chemical shift values according to the numbering of the atoms shown in Fig. 8. Table 13 shows the comparison with the experimental values (the full experimental spectrum is available in reference [80]). The absolute values are presented in ppm. The difference between the theoretical and experimental spectra are presented in the fourth column [80]. We corrected the possible deviations observed in the theoretical data with a scaling factor [106].

The chemical shifts lay within the expected range. Some points are worth highlighting: the signal due to C1 emerged between 185 and 220 ppm, corresponding to the ketone range; the signal due to C2 to C7 appeared between 110 and 175 ppm, indicating the presence of aromatic carbons; and the signal due to C11 arose between 8 and 30 ppm, attributed to R-CH_3. C8 showed an overestimated value, a behavior that has already been reported in the literature [105]. Nevertheless, we correlated the theoretical and experimental values in a linear regression graph (Supporting Information). The R^2 value was 0.9956, and the RMSE (root-mean-square error) value was 3.6, indicating good similarity between the data. The statistical parameters to correlate the data indicated a good trend between the responses. In cases where there was a greater difference between the responses, the theoretical data corresponded to the chemical shifts present in the expected experimental ranges. We emphasize that these differences can also be found between experimental data from different sources. This is due to several factors of solvents and matrix. That is why regions and not point values are used [93,107]. Table 14 shows the hydrogen chemical shift results for α-PVP HCl.

The linear regression graph (Supporting Information) yielded a correlation coefficient of 0.9834 between the theoretical and experimental data, and the RMSE value was 0.2. Although this value was lower than expected, the chemical shifts were within the expected range, showing good correspondence. The chemical shifts of the hydrogens corresponding to the aromatic chain emerged within the expected range: 6.5–8 ppm for H3 and H5 (meta), 6–10 ppm for H2 and H6 (ortho), and 7.3–8 ppm for H4 (para). In addition, the signals for the hydrogens H12, H13, and H14, corresponding to the methyl group, were found between 0.7 and 1.3 ppm, confirming the similarity between the results. Table 15 lists the carbon chemical shift results for α-PVP. However, in this case, we analyzed results for the free base.

The R^2 value obtained by the linear regression graph (Supporting Information) was 0.9965, and the RMSE value was 4.3. Despite the strong correspondence, the theoretical values diverged from the experimental ones. We analyzed the same structure (free-base), but this time we obtained the hydrogen chemical shifts results summarized in Table 16.

The R^2 value of the linear regression graph between the experimental and theoretical results was 0.9750, indicating that the results obtained by the simulation were closely correlated with the experimental values. The RMSE value was 0.49.

If we consider that during experimental procedures many variables compromise the accuracy of the results (e.g., errors of the analyst and equipment), the proposed method stands out for its reproducibility, among other factors, despite the problems highlighted previously.

Conclusion

This work achieved initially proposed the goals. The structural and spectroscopic properties evaluated through theoretical chemistry are comparable to the available experimental results. This proximity between the responses strengthens the potential of using these in silico techniques to obtain faster information for new psychoactive substances.

The conformers and the responses obtained by the Boltzmann distribution indicated that the crystallographic structure does not approximate the most probable structure by the conformational analysis. For this reason, we used the lowest energy structure and not the crystal available in the literature. To choose the best calculation conditions, a factorial design was performed. This approach aimed to choose the computational simulation method to be used with Flakka more assertively. The combination (B3LYP/6-31G**/D3BJ) showed the shortest computational time and the most significant similarity with the reference structure by RMSD.

The spectroscopic evaluation used experimental NMR (^1H and ^{13}C) and infrared data. Comparison between the experimental and simulated spectra showed high similarity for IR. This evaluation used linear regression of the wavelength values, and we also used HCA, PCA, and KL divergence. The NMR results were less similar when compared to the IR, as we observed overestimated ^{13}C NMR values for α-PVP HCl and α-PVP in the free-base form. These results were expected according to what has already been reported in the literature [108].

Given the combination of conformational analysis, factorial design, spectroscopic characterization, and comparison by statistical techniques, we have shown that in silico methods can provide information for substances that are still unknown or for which little information exists. Thus, using these techniques can help to optimize information gathering and can be a valuable ally in forensic matters.

CRediT authorship contribution statement

Tcharkhetian Adrinė Elisabeth Ganimian: Methodology, Formal analysis, Writing – original draft, Writing – review & editing, Visualization. **Bruni Aline Thais:** Conceptualization, Validation, Formal analysis, Resources, Writing – original draft, Writing – review & editing, Visualization, Project administration, Funding acquisition, Supervision. **Rodrigues Caio Henrique Pinke:** Conceptualization, Methodology, Validation, Formal analysis, Investigation, Writing – original draft, Writing – review & editing, Visualization, Project administration, Supervision.

Declaration of Competing Interest

The authors declare that they have no known competing financial interests or personal relationships that could have appeared to influence the work reported in this paper.

Acknowledgments

We thank Cynthia Prado Manso for language editing and proofreading and the Brazilian Agencies Conselho Nacional de Desenvolvimento Científico e Tecnológico (CNPq, grant 465450/2014-8) and Coordenação de Aperfeiçoamento de Pessoal de Nível Superior (CAPES, Finance Code 001) for financial support.

Appendix A. Supplementary data

Supplementary data to this article can be found online at https://doi.org/10.1016/j.rechem.2021.100254.

References

[1] J. Soares, V.M. Costa, M.d.L. Bastos, F. Carvalho, J.P. Capela, An updated review on synthetic cathinones, Arch. Toxicol. 95 (9) (2021) 2895–2940, https://doi.org/10.1007/s00204-021-03083-3.
[2] B. Potocka-Banaś, T. Janus, S. Majdanik, T. Banaś, T. Dembińska, K. Borowiak, Fatal Intoxication with α-PVP, a Synthetic Cathinone Derivative, J. Forensic Sci. 62 (2) (2017) 553–556, https://doi.org/10.1111/1556-4029.13326.
[3] A.B. Lopez-Rodriguez, M.-P. Viveros, Bath salts and polyconsumption: in search of drug-drug interactions, Psychopharmacology (Berl). 236 (3) (2019) 1001–1014, https://doi.org/10.1007/s00213-019-05213-3.
[4] L.-Y. Feng, A. Battulga, E. Han, H. Chung, J.-H. Li, New psychoactive substances of natural origin: A brief review, J. Food Drug Anal. 25 (3) (2017) 461–471, https://doi.org/10.1016/j.jfda.2017.04.001.

[5] United Nations Office on Drugs and Crime – UNODC, Current NPS Threats, Volume III, 1st ed., United Nations publication, Vienna, 2020.
[6] United Nations Office on Drugs and Crime – UNODC, Recommended methods for the Identification and Analysis of Synthetic Cathinones in Seized Materials (Revised and updated), (2020) 60.
[7] E. Bulska, R. Bachliński, M.K. Cyrański, M. Michalska-Kacymirow, W. Kośnik, P. Małecki, K. Grela, M.A. Dobrowolski, Comprehensive Protocol for the Identification and Characterization of New Psychoactive Substances in the Service of Law Enforcement Agencies, Front. Chem. 8 (2020) 693, https://doi.org/10.3389/fchem.2020.00693.
[8] Swgdrug, Recommendations for Code of Professional Practice, Education and Training, Methods of Analysis, and Quality Assurance, Sci. Work. Gr. Anal. Seized Drugs. (2019) 83.
[9] R. Houhou, T. Bocklitz, Trends in artificial intelligence, machine learning, and chemometrics applied to chemical data, Anal. Sci. Adv. 2 (3-4) (2021) 128–141.
[10] P.F. dos Santos, L.M. Souza, B.B. Merlo, H.B. Costa, L.V. Tose, H. Santos, G. Vanini, L.F. Machado, R.S. Ortiz, R.P. Limberger, B.G. Vaz, W. Romão, 2-(4-iodine-2,5-dimethoxyphenyl)-n-[(2-methoxyphenyl)methyl]etamine or 25I-NBOMEe: chemical characterization of a designer drug, Quim. Nova. 39 (2015) 229–237, https://doi.org/10.5935/0100-4042.20150178.
[11] A.E. Steuer, L. Brockbals, T. Kraemer, Metabolomic Strategies in Biomarker Research – New Approach for Indirect Identification of Drug Consumption and Sample Manipulation in Clinical and Forensic Toxicology? Front. Chem. 7 (2019) 1–24, https://doi.org/10.3389/fchem.2019.00319.
[12] L. Liu, S.E. Wheeler, R. Venkataramanan, J.A. Rymer, A.F. Pizon, M.J. Lynch, K. Tamama, Newly emerging drugs of abuse and their detection methods: An ACLPS critical review, Am. J. Clin. Pathol. 149 (2018) 105–116, https://doi.org/10.1093/AJCP/AQX138.
[13] C.H.P. Rodrigues, A.T. Bruni, In silico toxicity as a tool for harm reduction: A study of new psychoactive amphetamines and cathinones in the context of criminal science, Sci. Justice. 59 (3) (2019) 234–247, https://doi.org/10.1016/j.scijus.2018.11.006.
[14] M. Katselou, I. Papoutsis, P. Nikolaou, C. Spiliopoulou, S. Athanaselis, α-PVP ("flakka"): a new synthetic cathinone invades the drug arena, Forensic Toxicol. 34 (1) (2016) 41–50, https://doi.org/10.1007/s11419-015-0298-1.
[15] C.J. Groombridge, NMR Spectroscopy in Forensic Science, in: Annu. Reports NMR Spectrosc., 1996: pp. 215–297. https://doi.org/10.1016/S0066-4103(08)60080-0.
[16] C.A.F. De Oliveira Penido, M.T.T. Pacheco, I.K. Lednev, L. Silveira, Raman spectroscopy in forensic analysis: Identification of cocaine and other illegal drugs of abuse, J. Raman Spectrosc. 47 (2016) 28–38, https://doi.org/10.1002/jrs.4864.
[17] R. Risoluti, S. Materazzi, A. Gregori, L. Ripani, Early detection of emerging street drugs by near infrared spectroscopy and chemometrics, Talanta. 153 (2016) 407–413, https://doi.org/10.1016/j.talanta.2016.02.044.
[18] K.E. Kongshaug, S. Pedersen-Bjergaard, K.E. Rasmussen, M. Krogh, Solid-phase microextraction/capillary gas chromatography for the profiling of confiscated ecstacy and amphetamine, Chromatographia. 50 (3-4) (1999) 247–252, https://doi.org/10.1007/BF02490660.
[19] A. Sorribes-Soriano, F.A. Esteve-Turrillas, S. Armenta, P. Amorós, J.M. Herrero-Martínez, Amphetamine-type stimulants analysis in oral fluid based on molecularly imprinting extraction, Anal. Chim. Acta. 1052 (2019) 73–83, https://doi.org/10.1016/j.aca.2018.11.046.
[20] M. Morelato, A. Beavis, M. Tahtouh, O. Ribaux, P. Kirkbride, C. Roux, The use of forensic case data in intelligence-led policing: The example of drug profiling, Forensic Sci. Int. 226 (1-3) (2013) 1–9, https://doi.org/10.1016/j.forsciint.2013.01.003.
[21] G.C. Terstappen, A. Reggiani, In silico research in drug discovery, Trends Pharmacol. Sci. 22 (1) (2001) 23–26, https://doi.org/10.1016/S0165-6147(00)01584-4.
[22] A.B. Raies, V.B. Bajic, In silico toxicology: computational methods for the prediction of chemical toxicity, Wiley Interdiscip. Rev. Comput. Mol. Sci. 6 (2) (2016) 147–172, https://doi.org/10.1002/wcms.1240.
[23] V. Alves, R. Braga, E. Muratov, C. Andrade, QUIMIOINFORMÁTICA: UMA INTRODUÇÃO, Quim. Nova. 41 (2017) 202–212, https://doi.org/10.21577/0100-4042.20170145.
[24] H.J. Kulik, M.S. Sigman, Advancing Discovery in Chemistry with Artificial Intelligence: From Reaction Outcomes to New Materials and Catalysts, Acc. Chem. Res. 54 (10) (2021) 2335–2336, https://doi.org/10.1021/acs.accounts.1c00232.
[25] L. He, L.u. Bai, D.D. Dionysiou, Z. Wei, R. Spinney, C. Chu, Z. Lin, R. Xiao, Applications of computational chemistry, artificial intelligence, and machine learning in aquatic chemistry research, Chem. Eng. J. 426 (2021) 131810, https://doi.org/10.1016/j.cej.2021.131810.
[26] M. Vujović, V. Ragavendran, B. Arsić, E. Kostić, M. Mladenović, DFT calculations as an efficient tool for prediction of Raman and infra-red spectra and activities of newly synthesized cathinones, Open Chem. 18 (2020) 185–195, https://doi.org/10.1515/chem-2020-0021.
[27] J.A. de Sousa, F. Ivan, Explorando a Química Computacional, 1st ed., Simplissimo Livros Ltda, Teresina, 2021.
[28] C.M.R. Sant'Anna, Molecular modeling methods in the study and design of bioactive compounds: An introduction, Rev. Virtual Química. 1 (2009) 49–57. https://doi.org/10.5935/1984-6835.20090007.
[29] P.A. Fantin, Conjunto de Bases Gaussianas de Qualidade Tripla Zeta de Valência para Funções de Onda Correlacionadas, Universidade Federal do Espírito Santo, 2007. http://www.dominiopublico.gov.br/pesquisa/DetalheObraForm.do?select_action=&co_obra=202060.
[30] M. Ali, A. Mansha, S. Asim, M. Zahid, M. Usman, N. Ali, DFT Study for the Spectroscopic and Structural Analysis of p-Dimethylaminoazobenzene, J. Spectrosc. 2018 (2018) 1–15, https://doi.org/10.1155/2018/9365153.
[31] V.K. Shukla, M.A. Al-Alshaikh, A.A. El-Emam, A.K. Sachan, R. Srivastava, O. Prasad, L. Sinha, Conformational search, spectral analysis and electronic properties of 5-(4-Pyridinyl)-1,3,4-thiadiazol-2-amine, J. Mol. Struct. 1108 (2016) 112–125, https://doi.org/10.1016/j.molstruc.2015.11.077.
[32] Toby Lewis-Atwell, Piers A. Townsend, Matthew N. Grayson, Comparisons of different force fields in conformational analysis and searching of organic molecules: A review, Tetrahedron. 79 (2021) 131865, https://doi.org/10.1016/j.tet.2020.131865.
[33] Renzhi Chen, Yang Shen, Sihan Yang, Yandong Zhang, Conformational Design Principles in Total Synthesis, Angew. Chemie Int. Ed. 59 (34) (2020) 14198–14210, https://doi.org/10.1002/anie.202003735.
[34] A.R. Leach, Molecular Modelling: Principles and Applications, 2nd ed., Prentice Hall, England, 2001.
[35] Aline Thais Bruni, Márcia Miguel Castro Ferreira, Theoretical study of omeprazole behavior: Racemization barrier and decomposition reaction, Int. J. Quantum Chem. 108 (6) (2008) 1097–1106, https://doi.org/10.1002/qua.21597.
[36] R. Vafazadeh, M. Namazian, M. Chavoshiyan, A.C. Willis, P.D. Carr, Synthesis, X-ray Structural Characterization, and DFT Calculations of Binuclear Mixed-ligand Copper(II) Complexes Containing Diamine, Acetate and Methacrylate Ligands, Acta Chim. Slov. (2017) 613–620, https://doi.org/10.17344/acsi.2017.3401.
[37] S. Lahmidi, E.H. Anouar, L. El Hamdaoui, Y. Ouzidan, M. Kaur, J.P. Jasinski, N. K. Sebbar, E.M. Essassi, M. El Moussaouiti, Synthesis, crystal structure, spectroscopic characterization, hirshfeld surface analysis, DFT calculations and antibacterial activity of ethyl 2-(4-vinylbenzyl)-2-(5-methyl-[1,2,4]triazolo[1,5-a]pyrimidin-7-yl)-3-(4-vinylphenyl)propanoate, J. Mol. Struct. 1191 (2019) 66–75, https://doi.org/10.1016/j.molstruc.2019.04.076.
[38] J. Lim, M. Szymczyk, N. Mehraban, Y. Ding, L. Parrillo-Chapman, A. El-Shafei, H. S. Freeman, Data from X-ray crystallographic analysis and DFT calculations on isomeric azo disperse dyes, Data Br. 21 (2018) 675–683, https://doi.org/10.1016/j.dib.2018.10.010.
[39] J. Lim, M. Szymczyk, N. Mehraban, Y. Ding, L. Parrillo-Chapman, A. El-Shafei, H. S. Freeman, Molecular and excited state properties of isomeric scarlet disperse dyes, J. Mol. Struct. 1161 (2018) 254–261, https://doi.org/10.1016/j.molstruc.2018.02.028.
[40] Zbigniew A. Dreger, Adam I. Stash, Zhi-Gang Yu, Yu-Sheng Chen, Yuchuan Tao, Yogendra M. Gupta, High-Pressure Crystal Structures of an Insensitive Energetic Crystal: 1,1-Diamino-2,2-dinitroethene, J. Phys. Chem. C. 120 (2) (2016) 1218–1224, https://doi.org/10.1021/acs.jpcc.5b10644.10.1021/acs.jpcc.5b10644.s001.
[41] M.D. Hanwell, D.E. Curtis, D.C. Lonie, T. Vandermeersch, E. Zurek, G. R. Hutchison, Avogadro: an advanced semantic chemical editor, visualization, and analysis platform, J. Cheminform. 4 (2012) 17, https://doi.org/10.1186/1758-2946-4-17.
[42] A.K. Rappe, C.J. Casewit, K.S. Colwell, W.A. Goddard, W.M. Skiff, UFF, a full periodic table force field for molecular mechanics and molecular dynamics simulations, J. Am. Chem. Soc. 114 (25) (1992) 10024–10035, https://doi.org/10.1021/ja00051a040.
[43] Frank Neese, Software update: the ORCA program system, version 4.0, WIREs Comput, Mol. Sci. 8 (1) (2018), https://doi.org/10.1002/wcms.2018.8.issue-110.1002/wcms.1327.
[44] W. Kohn, L.J. Sham, Self-Consistent Equations Including Exchange and Correlation Effects, Phys. Rev. 140 (4A) (1965) A1133–A1138, https://doi.org/10.1103/PhysRev.140.A1133.
[45] Axel D. Becke, Density-functional thermochemistry. III. The role of exact exchange, J. Chem. Phys. 98 (7) (1993) 5648–5652, https://doi.org/10.1063/1.464913.
[46] Chengteh Lee, Weitao Yang, Robert G. Parr, Development of the Colle-Salvetti correlation-energy formula into a functional of the electron density, Phys. Rev. B. 37 (2) (1988) 785–789, https://doi.org/10.1103/PhysRevB.37.785.
[47] Michael J. Frisch, John A. Pople, J. Stephen Binkley, Self-consistent molecular orbital methods 25. Supplementary functions for Gaussian basis sets, J. Chem. Phys. 80 (7) (1984) 3265–3269, https://doi.org/10.1063/1.447079.
[48] K. AZOUZI, B. HAMDI, R. ZOUARI, A. BEN SALAH, Synthesis, structure and Hirshfeld surface analysis, vibrational and DFT investigation of (4-pyridine carboxylic acid) tetrachlorocuprate (II) monohydrate, Bull. Mater. Sci. 40 (2017) 289–299. https://doi.org/10.1007/s12034-017-1375-3.
[49] Youness El Bakri, Lei Guo, El Hassane Anouar, Abdallah Harmaoui, Abdelkader Ben Ali, El Mokhtar Essassi, Joel T. Mague, Synthesis, crystal structure, DFT, molecular dynamics simulation and evaluation of the anticorrosion performance of a new pyrazolotriazole derivative, J. Mol. Struct. 1176 (2019) 290–297, https://doi.org/10.1016/j.molstruc.2018.08.107.
[50] William Humphrey, Andrew Dalke, Klaus Schulten, VMD: Visual molecular dynamics, J. Mol. Graph. 14 (1) (1996) 33–38, https://doi.org/10.1016/0263-7855(96)00018-5.
[51] Tamara Husch, Dieter Seebach, Albert K. Beck, Markus Reiher, Rigorous Conformational Analysis of Pyrrolidine Enamines with Relevance to Organocatalysis, Helv. Chim. Acta. 100 (10) (2017) e1700182, https://doi.org/10.1002/hlca.v100.1010.1002/hlca.201700182.
[52] D. Granato, J.S. Santos, G.B. Escher, B.L. Ferreira, R.M. Maggio, Use of principal component analysis (PCA) and hierarchical cluster analysis (HCA) for

multivariate association between bioactive compounds and functional properties in foods: A critical perspective, Trends Food Sci. Technol. 72 (2018) 83–90, https://doi.org/10.1016/j.tifs.2017.12.006.
[53] I. Nahum-Shani, J.J. Dziak, L.M. Collins, Multilevel factorial designs with experiment-induced clustering, Psychol. Methods. 23 (2018) 458–479, https://doi.org/10.1037/met0000128.
[54] D.R. Burgard, J.T. Kuznicki, Chemometrics: Chemical and Sensory Data, 1st ed., CRC Press, 2018. https://doi.org/10.1201/9781351070607.
[55] Ramakrishna Gottipati, Susmita Mishra, Process optimization of adsorption of Cr (VI) on activated carbons prepared from plant precursors by a two-level full factorial design, Chem. Eng. J. 160 (1) (2010) 99–107, https://doi.org/10.1016/j.cej.2010.03.015.
[56] Jorge L. Brasil, Lucas C. Martins, Ricardo R. Ev, Jairton Dupont, Sívio L.P. Dias, José A.A. Sales, Cláudio Airoldi, Éder C. Lima, Factorial design for optimization of flow-injection preconcentration procedure for copper(II) determination in natural waters, using 2-aminomethylpyridine grafted silica gel as adsorbent and spectrophotometric detection, Int. J. Environ. Anal. Chem. 85 (7) (2005) 475–491, https://doi.org/10.1080/03067310500117350.
[57] A.H.C. Horn, Essentials of Computational Chemistry, Theories and Models, J. Chem. Inf. Comput. Sci. 43 (2003) 1720–1720. https://doi.org/10.1021/ci010445m.
[58] D.C. Young, Computational Chemistry, 1st ed., John Wiley & Sons, Inc., New York, USA, 2001. https://doi.org/10.1002/0471220655.
[59] Manoj K. Kesharwani, Brina Brauer, Jan M.L. Martin, Frequency and Zero-Point Vibrational Energy Scale Factors for Double-Hybrid Density Functionals (and Other Selected Methods): Can Anharmonic Force Fields Be Avoided? J. Phys. Chem. A. 119 (9) (2015) 1701–1714, https://doi.org/10.1021/jp508422u.
[60] Stefan Grimme, Stephan Ehrlich, Lars Goerigk, Effect of the damping function in dispersion corrected density functional theory, J. Comput. Chem. 32 (7) (2011) 1456–1465, https://doi.org/10.1002/jcc.21759.
[61] Stefan Grimme, Jens Antony, Stephan Ehrlich, Helge Krieg, A consistent and accurate ab initio parametrization of density functional dispersion correction (DFT-D) for the 94 elements H-Pu, J. Chem. Phys. 132 (15) (2010) 154104, https://doi.org/10.1063/1.3382344.
[62] Seiji Tsuzuki, Tadafumi Uchimaru, Accuracy of intermolecular interaction energies, particularly those of hetero-atom containing molecules obtained by DFT calculations with Grimme's D2, D3 and D3BJ dispersion corrections, Phys. Chem. Chem. Phys. 22 (39) (2020) 22508–22519, https://doi.org/10.1039/D0CP03679J.
[63] M.M.C. Ferreira, QUIMIOMETRIA – Conceitos, Métodos e Aplicações, 1st ed., Editora da Unicamp, Campinas, 2015.
[64] Matthew R. Wood, Ivan Bernal, Roger A. Lalancette, The dangerous new synthetic drug α-PVP as the hydrated chloride salt α-pyrrolidinopentiophenone hydrochloride 0.786-hydrate, Acta Crystallogr, Sect. C Struct. Chem. 72 (1) (2016) 48–51, https://doi.org/10.1107/S2053229615023621.
[65] Joseph M Hilbe, STATISTICA 7, Am. Stat. 61 (1) (2007) 91–94, https://doi.org/10.1198/000313007X172998.
[66] Karel G. von Eschwege, Jeanet Conradie, Annemarie Kuhn, Dithizone and Its Oxidation Products: A DFT, Spectroscopic, and X-ray Structural Study, J. Phys. Chem. A. 115 (51) (2011) 14637–14646, https://doi.org/10.1021/jp208212e.
[67] Biswajit Mandal, Shamik Chakrabarti, Awalendra K. Thakur, DFT simulation of NaFeSnO4 structure, electronic and electrochemical properties validated by experimental results, Comput. Mater. Sci. 192 (2021) 110401, https://doi.org/10.1016/j.commatsci.2021.110401.
[68] F. Sen, I. Yilmaz, M. Dinçer, A. Cukurovali, STRUCTURAL FEATURES OF 2-(4,5-DIPHENYL-4H-1,2,4-TRIAZOL-3-YL)THIO)-1-(3-METHYL-3-PHENYLCYCLOBUTYL) ETHANONE: X-RAY DIFFRACTION AND DFT CALCULATIONS, J. Chil. Chem. Soc. 60 (2015) 2671–2676, https://doi.org/10.4067/S0717-97072015000400009.
[69] Muhammad Khalid, Malik Aman Ullah, Muhammad Adeel, Muhammad Usman Khan, Muhammad Nawaz Tahir, Ataualpa Albert Carmo Braga, Synthesis, crystal structure analysis, spectral IR, UV–Vis, NMR assessments, electronic and nonlinear optical properties of potent quinoline based derivatives: Interplay of experimental and DFT study, J. Saudi Chem. Soc. 23 (5) (2019) 546–560, https://doi.org/10.1016/j.jscs.2018.09.006.
[70] T.M. Buriol, M.A. Argenta, ACELERANDO O DESENVOLVIMENTO E O PROCESSAMENTO DE ANÁLISES NUMÉRICAS COMPUTACIONAIS UTILIZANDO PYTHON E CUDA, Curitiba, 2009. https://www.researchgate.net/publication/228683446_ACELERANDO_O_DESENVOLVIMENTO_EO_PROCESSAMENTO_DE_ANALISES_NUMERICAS_COMPUTACIONAIS_UTILIZANDO_PYTHON_E_CUDA.
[71] G. van Rossum, F.L. Drake, The Python Language Reference Manual, 1st ed.,, Network Theory, 2011.
[72] J. VanderPlas, Python Data Science Handbook: Essential Tools for Working with Data, 1st ed.,, O'Reilly Media Inc, 2016.
[73] Travis E. Oliphant, Python for Scientific Computing, Comput. Sci. Eng. 9 (3) (2007) 10–20, https://doi.org/10.1109/MCSE.2007.58.
[74] A. Masad, F. Masad, H. Odeh, Repl.it, Replit Inc. (2016). https://replit.com/ (accessed November 6, 2021).
[75] A.T. Bruni, P.O.M. de Carvalho, C.H.P. Rodrigues, V.B.P. Leite, In silico methods in forensic science: Quantum chemistry and multivariate analysis applied to infrared spectra of new amphetamine- and cathinone-derived psychoactive substances, Forensic Chem. 9 (2018) 21–34, https://doi.org/10.1016/j.forc.2018.03.006.
[76] Marie L. Laury, Matthew J. Carlson, Angela K. Wilson, Vibrational frequency scale factors for density functional theory and the polarization consistent basis sets, J. Comput. Chem. 33 (30) (2012) 2380–2387, https://doi.org/10.1002/jcc.23073.
[77] NIST Standard Reference Database 101, Computational Chemistry Comparison and Benchmark DataBase, Release 18, Natl. Inst. Stand. Technol. (2016).
[78] Vincenzo Barone, Maurizio Cossi, Quantum Calculation of Molecular Energies and Energy Gradients in Solution by a Conductor Solvent Model, J. Phys. Chem. A. 102 (11) (1998) 1995–2001, https://doi.org/10.1021/jp9716997.
[79] Yu Takano, K.N. Houk, Benchmarking the Conductor-like Polarizable Continuum Model (CPCM) for Aqueous Solvation Free Energies of Neutral and Ionic Organic Molecules, J. Chem. Theory Comput. 1 (1) (2005) 70–77, https://doi.org/10.1021/ct049977a10.1021/ct049977a.s001.
[80] J.F. Casale, P.A. Hays, The Characterization of α-Pyrrolidinopentiophenone, Microgram J. 9 (2012) 33–38. https://deagovdev.dea.gov/sites/default/files/pr/microgram-journals/2012/mj9-1_33-38.pdf.
[81] P.W. Atkins, R. Friedman, Molecular Quantum Mechanics, Quantum. 134 (2011) 588.
[82] Ajoy Kumer, Md. Wahab Khan, The effect of alkyl chain and electronegative atoms in anion on biological activity of anilinium carboxylate bioactive ionic liquids and computational approaches by DFT functional and molecular docking, Heliyon. 7 (7) (2021) e07509, https://doi.org/10.1016/j.heliyon.2021.e07509.
[83] Manos C. Vlasiou, Kyriaki S. Pafti, Screening possible drug molecules for Covid-19. The example of vanadium (III/IV/V) complex molecules with computational chemistry and molecular docking, Comput. Toxicol. 18 (2021) 100157, https://doi.org/10.1016/j.comtox.2021.100157.
[84] Dita Spálovská, Martin Paškan, Bronislav Jurásek, Martin Kuchař, Michal Kohout, Vladimír Setnička, Structural spectroscopic study of enantiomerically pure synthetic cathinones and their major metabolites, New J. Chem. 45 (2) (2021) 850–860, https://doi.org/10.1039/D0NJ05065B.
[85] Shovkatjon Akhunov, Khatam Ashurov, Sherzod Axmedov, Beknazar Kasimov, Vladimir Rotshteyn, Azim Radjabov, Dilshadbek Usmanov, Development of surface ionization mass spectrometry for detection of stimulants in human urine, Eur. J. Mass Spectrom. 27 (1) (2021) 29–38, https://doi.org/10.1177/14690667211002777.
[86] Akash Ghosh, Gourisankar Roymahapatra, Debarati Paul, Santi M. Mandal, Theoretical analysis of bacterial efflux pumps inhibitors: Strategies in-search of competent molecules and develop next, Comput. Biol. Chem. 87 (2020) 107275, https://doi.org/10.1016/j.compbiolchem.2020.107275.
[87] Kevin E. Riley, Kenneth M. Merz, Assessment of Density Functional Theory Methods for the Computation of Heats of Formation and Ionization Potentials of Systems Containing Third Row Transition Metals, J. Phys. Chem. A. 111 (27) (2007) 6044–6053, https://doi.org/10.1021/jp070593110.1021/jp0705931.s00110.1021/jp0705931.s00210.1021/jp0705931.s00310.1021/jp0705931.s004.
[88] M.A. Spackman, A.S. Mitchell, Basis set choice and basis set superposition error (BSSE) in periodic Hartree-Fock calculations on molecular crystals, Phys. Chem. Chem. Phys. 3 (2001) 1518–1523, https://doi.org/10.1039/b009159f.
[89] Dmitrij Rappoport, Filipp Furche, Property-optimized Gaussian basis sets for molecular response calculations, J. Chem. Phys. 133 (13) (2010) 134105, https://doi.org/10.1063/1.3484283.
[90] Michael F. Peintinger, Daniel Vilela Oliveira, Thomas Bredow, Consistent Gaussian basis sets of triple-zeta valence with polarization quality for solid-state calculations, J. Comput. Chem. 34 (6) (2013) 451–459, https://doi.org/10.1002/jcc.23153.
[91] Florian Weigend, Reinhart Ahlrichs, Balanced basis sets of split valence, triple zeta valence and quadruple zeta valence quality for H to Rn: Design and assessment of accuracy, Phys. Chem. Chem. Phys. 7 (18) (2005) 3297, https://doi.org/10.1039/b508541a.
[92] (SWGDRUG) Scientific Working Group for the Analysis of Seized Drugs, SWGDRUG Recommendations Version 7.1, United States Departament of Justice, Washington DC, USA, 2016.
[93] D.L. Pavia, G.M. Lampman, G.S. Kriz, J.A. Vyvyan, Introduction to Spectroscopy, 4th ed, Cengage Learning, 2008.
[94] K.R. Beebe, R.J. Pell, M.B. Seasholtz, Chemometrics: A Practical Guide, 1st ed., John Wiley & Sons Inc, 1998.
[95] J. Miller, J.C. Miller, R.D. Miller, Statistics and Chemometrics for Analytical Chemistry, 7th ed.,, Pearson Education Limited, 2018.
[96] R.G. Brereton, Chemometrics, 1st ed., John Wiley & Sons, Ltd, Chichester, UK, 2003. https://doi.org/10.1002/0470863242.
[97] Tim van Erven, Peter Harremoes, Rényi Divergence and Kullback-Leibler Divergence, IEEE Trans. Inf. Theory. 60 (7) (2014) 3797–3820, https://doi.org/10.1109/TIT.2014.2320500.
[98] S. Ji, Z. Zhang, S. Ying, L. Wang, X. Zhao, Y. Gao, Kullback-Leibler Divergence Metric Learning, IEEE Trans. Cybern. (2020) 1–12, https://doi.org/10.1109/TCYB.2020.3008248.
[99] L.O. Ahmed, R.A. Omer, A Theoretical Study on Dopamine Molecule, J. Phys. Chem. Funct. Mater. 2 (2019) 66–72. https://dergipark.org.tr/en/download/article-file/887407.
[100] Hélio F. Dos Santos, Marcelo A. Chagas, Leonardo A. De Souza, Willian R. Rocha, Mauro V. De Almeida, Cleber P.A. Anconi, Wagner B. De Almeida, Water Solvent Effect on Theoretical Evaluation of 1 H NMR Chemical Shifts: o -Methyl-Inositol Isomer, J. Phys. Chem. A. 121 (14) (2017) 2839–2846, https://doi.org/10.1021/acs.jpca.7b0106710.1021/acs.jpca.7b01067.s001.
[101] Haroldo C. Da Silva, Wagner B. De Almeida, Theoretical calculations of 1H NMR chemical shifts for nitrogenated compounds in chloroform solution, Chem. Phys. 528 (2020) 110479, https://doi.org/10.1016/j.chemphys.2019.110479.

[102] J. Kujawski, K. Czaja, K. Dettlaff, J. Żwawiak, T. Ratajczak, M.K. Bernard, Structural and spectroscopic properties of posaconazole – Experimental and theoretical studies, J. Mol. Struct. 1181 (2019) 179–189, https://doi.org/10.1016/j.molstruc.2018.12.074.

[103] Rodrigo N. Guzzo, Michelle Jakeline Cunha Rezende, Vinicius Kartnaller, José Walkimar de M. Carneiro, Stanislav R. Stoyanov, Leonardo Moreira da Costa, Experimental and DFT evaluation of the 1H and 13C NMR chemical shifts for calix[4]arenes, J. Mol. Struct. 1157 (2018) 97–105, https://doi.org/10.1016/j.molstruc.2017.12.038.

[104] Züleyha Özer, Turgut Kılıç, Sema Çarıkçı, Akın Azizoglu, Synthesis, Structural Characterization, Spectroscopic Properties, and Theoretical Investigation of Siderol Acetate, Russ. J. Phys. Chem. A. 93 (13) (2019) 2703–2709, https://doi.org/10.1134/S0036024419130235.

[105] Rupal Jain, Thomas Bally, Paul R. Rablen, Calculating Accurate Proton Chemical Shifts of Organic Molecules with Density Functional Methods and Modest Basis Sets, J. Org. Chem. 74 (11) (2009) 4017–4023, https://doi.org/10.1021/jo900482q.

[106] Cem Cüneyt Ersanli, Günay Kaya Kantar, Selami Şaşmaz, Crystallographic, spectroscopic (FTIR and NMR) and quantum computational calculation studies on bis(2-methoxy-4-((E)-prop-1-enyl)phenyl)oxalate, J. Mol. Struct. 1143 (2017) 318–327, https://doi.org/10.1016/j.molstruc.2017.04.032.

[107] H. Günther, NMR Spectroscopy: Basic Principles, Concepts ans Applications in Chemistry, 3rd ed.,, John Wiley and Sons Ltd, 2013.

[108] Paola Cimino, Luigi Gomez-Paloma, Dario Duca, Raffaele Riccio, Giuseppe Bifulco, Comparison of different theory models and basis sets in the calculation of 13C NMR chemical shifts of natural products, Magn. Reson. Chem. 42 (S1) (2004) S26–S33, https://doi.org/10.1002/mrc.1410.